July-August 2020
ISSN: 0193-4120 Page No. 3035 - 3052

CLASSIFYING VARIOUS BRAIN ACTIVITIES BY EXPLOITING DEEP LEARNING TECHNIQUES AND GENETIC ALGORITHM FUSION METHOD

Marwa Mawfaq MohamedSheet AL-Hatab[1,2], Raid Rafi Omar Al-Nima[2], Ilaria Marcantoni[1], Camillo Porcaro[1,3,4,5,6] and Laura Burattini[1]

[1]Department of Information Engineering, Università Politecnica delle Marche, Ancona, Italy
[2]Technical Engineering College / Northern Technical University / Iraq
[3]Institute of Cognitive Sciences and Technologies (ISTC) - National Research Council (CNR), Rome, Italy
[4]S. Anna Institute and Research in Advanced Neurorehabilitation (RAN) Crotone, Italy
[5]Research Center for Motor Control and Neuroplasticity, KU Leuven, Leuven, Belgium
[6]Centre for Human Brain Health, School of Psychology, University of Birmingham, Birmingham, United Kingdom

Article Info
Page Number: 3035 - 3052
Publication Issue:
July-August 2020
Do not Edit

Article History
Article Received: *3 January 2019*
Revised: *25 March 2019*
Accepted: *28 July 2019*
Publication: *20 October 2019*

Abstract

The scan of functional Magnetic Resonance Imaging (fMRI) can provide three views for brain activities. These views are basically the X_axis (sagittal Plane), Y_axis (coronal plane) and Z_axis (axial plane). To the best of the obtained knowledge, studying brain activities for all of these views has not been considered before together with Deep Learning (DL) techniques. In this paper, various DL models named the X_axis Classification Model (XCM), Y_axis Classification Model (YCM) and Z_axis Classification Model (ZCM) are proposed. Each of these models is able to classify between the vision, movement and forward brain activities. Extensive experiments are performed for examining their parameters. The designed models have the capability to automatically detect the important features without any human supervision. In addition, they can provide intelligent decisions or classifications. Furthermore, effective combination method is suggested based on the Genetic Algorithm (GA) and Genetic Weighted Summation (GWS) rule, where high performances of outcomes can be achieved. After extensive experiments, the accuracies of 91.67%, 89.88% and 91.67% have been obtained for the XCM, YCM and ZCM, respectively. In addition, the accuracy has been raised to 97.22% by applying the suggested fusion method.
.

Keywords: *Brain Activities, Classification, Deep Learning, Functional Magnetic Resonance Imaging, Genetic Algorithm*

I. Introduction

Brain is one of the most mysterious organs in human‘s body. It is complex and very important. In recent decades and through the impressive technological progress, the brain structure has been discovered to involve three main parts: forebrain, midbrain and hindbrain. Each part has specific function. The brain can control human‘s body through a nervous system. Without the nervous system, rest of organs cannot perform their functions in the appropriate manner. In other words, the brain determines the way that each organ within the personal body works even in coordinating to other organs. There are more than ten billion cells that are connected with each other to receive, transmit and process the messages between cells. The messages can be sent from and to all parts of a body. They also control vital functions and tasks such as memory, behavior, emotion and thought, in addition to consider basic life functions such as heart rate

July-August 2020
ISSN: 0193-4120 Page No. 3035 - 3052

and breathing [1] [2] [3]. Knowledge about the brain is now more than before (e.g. the beginning of the nineteenth century), thanks to the developments of measuring devices of brain cues and functions. Neuroimaging is an example of brain measuring techniques. Neuroimaging is a common name for several methods that allow visualizing structures, functions and biochemical characteristics of the brain [4]. In recent years, the topic of brain signal analysis has become very popular in neuroscience. At the same time, neuroimaging techniques do not require surgical intervention or direct contact with the internal organs. Therefore, it is possible for non-invasive visualizations of brain structure and functionality to become powerful tools for researches and medical diagnostics after the developments of technologies and computational methods. Neuroimaging is a new system that aids medicine, psychology and neuroscience. Physicians who specify the presentation and interpretation of neuroimaging in the clinical site are known as neuroradiologists. Neuroimaging falls into two general categories: the first category is the structural imaging, it refers to the specialized approaches that visualize and analyze the anatomical properties of the brain. In addition, it helps in diagnosing a large-scale of intracranial medical cases as tumor or injury. The second category is the functional imaging, it is used to identify brain regions and highlighting brain processes that are associated with performing specific cognitive or behavioral tasks. Also, it allows determining development injuries and diseases such as Alzheimer‘s disease. Neurological imaging is also used to explain brain map activities of motor, sensory, cognitive and emotional tasks for individuals [5].

Neuroimaging includes many common types that are useful for collecting and analyzing personal brain images. They are as follows [6]: Computed Tomography (CT) scan, Magnetoencephalography (MEG), Electroencephalography (EEG), Stereotactic EEG (SEEG), Electrocorticography (ECoG), Positron Emission Tomography (PET), Single Photon Emission Computed Tomography (SPECT), Near-Infrared Spectroscopy (nIRS), Magnetic Resonance Imaging (MRI) and fMRI.

The fMRI imaging technique is more safer than the others. There are no known big risks from exposing the magnetic fields and radio waves. In contrary, the PET, SPECT and CT have some dangerous effects. In PET and SPECT, the radioactive decay production of gamma rays forms an electromagnetic radiation. But with a high amount of energy, this may cause danger effects to human‘s body. Similarly, the CT uses ionization radiation for the X-ray to provide brain structures as the MRI. The MEG signals are extremely small, so, several other signals in a typical environment can obscure these signals out of the brain. They also have very long time scales. SEEG and ECoG have set of limitations, where they are used in clinical settings at few hospitals and only doable by special trained teams of investigators and clinicians. Moreover, the locations of electrodes are clinically decided. Then, surgical intervention is required for implanting the electrodes into a brain. Once this is done, they cannot be changed in order to reduce the patient's vulnerability to the risks of surgery. For that reason the investigator cannot penetrate the cortex many times to find the responsive neurons. The EEG and nIRS do not provide enough information and high accurate outcomes as can be obtained by the fMRI [**6**]. On the other hand, the fMRI has good spatial resolutions, covers the whole brain and is particularly well adapted to localize the effects of brain activities. Its constructs brain maps and it can provide understanding the underlying brain connectivity. More recently, the fMRI technique has been applied to further understand the neurobehavioral disorders such as epilepsy, stroke, brain tumor, brain traumatic and multiple sclerosis. This can be achieved by scanning the brain activity while applying stimulations and recording the activity response of certain brain parts. Usually, it almost spends a very small time of 1-3 s for a spatial resolution of $1 - 3$ mm. It also allows better understanding of how the brain works. For all of the highlighted reasons, the fMRI can be considered as a powerful method for brain imaging [**7**]. The fMRI limitation can be presented by containing a number of data for each patient, which makes this challenging in the field of classification. Furthermore, it has high dimensions of hundreds or thousands of voxels, where this may cause delays in processing time [**8**].

This work is aiming to present a new scheme of recognizing various essential brain activities from fMRI images. More specifically, the vision, movement and forward activities are considered to be classified by the power of DL techniques. Comprehensive study will be provided by applying three types of views for each activity (the views of X_axis, Y_axis and Z_axis). In addition, the confidence of recognition will be enhanced by suggesting a fusion of Genetic Weighted Summation (GWS) strategy between the classified X_axis, Y_axis and Z_axis views.

The objectives and contributions of this work can be highlighted as follows:

1. Designing, evaluating and implementing efficient DL networks called the XCM, YCM and ZCM for the three axes views of X_axis, Y_axis and Z_axis, respectively. Each of these models is able to classify between the vision, movement and forward brain activities. Extensive experiments are performed for examining all proposed models parameters.
2. Enhancing the confidence of classification decision by employing the GWS fusing between the outcomes of the three axes views (X_axis, Y_axis and Z_axis). Also, comparing and analysing all the achieved performances.
3. To the best of the obtained knowledge this is the first comprehensive study that provides a new and full scheme of classifying the vision, movement and forward brain activities from the fMRI images. This can help doctors, researchers and medical carers in understanding personal neurons activities.

II. LITERATURE REVIEW

Previous studies that are related to this work can be reviewed as follows:

In 2014, Eslami and Saeed worked on the Attention Deficit Hyperactivity Disorder (ADHD) to classify the brain

July-August 2020
ISSN: 0193-4120 Page No. 3035 - 3052

disorders of children. The authors considered the similarity and dissimilarity between brain images. To recognize the ADHD from healthy individuals, Eigenvalues and Eigenvectors were calculated for the entire brain signals. Eextended Frobenius (Eros) normalization, which is denoted as a weighted cosine similarity between the pairs of Eigenvectors according to their corresponding Eigenvalues, was suggested to be the indicator of the similarity between brain images. Furthermore, the K-Nearest Neighbor method is utilized to classify between the healthy and unhealthy cases. It seems that the brain images of Z_axis view was used [**9**]. In 2014, Wang *et al.* described a classification algorithm for pediatric epilepsy using fMRI language_related activation maps. Their work was based on performing an auditory description decision task by each subject. Nearest_Neighbor Classifier (NNC) and Distance_Based Fuzzy Classifier (DFC) were used. The results on 122 real fMRI images show that 90 subjects gave similar classification results for all the employed tasks [**10**]. In 2015, Suhaimi *et al.* presented a study for classifying fMRI images by exploiting the Deep Learning (DL) technique. Comparisons were here established for the classification of ADHD, memory encoding, memory encoding, memory decoding and brain parcellation. It also seems that the Z_axis view images were utilized [11]. In 2017, Meszlényi *et al*. proposed a Connectome-Convolutional Neural Network (CCNN). This network can recognize the resting state from the fMRI images. Only the Z_axis view was employed in this work [12]. In 2018, Wen *et al*. investigated DL methods to process the fMRI data. The application of this study was performed for diagnosing the cognitive impairment. It appears that the Z_axis views were exploited [13]. In the same year, Pallares *et al.* suggested extracting multivariate signatures from a set of new standard fMRI data. The authors verify that informations of different modalities were not mixed. The authors recognized between different subjects of individuals. The authors also classified between the various behavioral conditions. This work was organized into two parts. Firstly, using coupled wholebrain Effective Connectivity (EC) estimation with adequate machine learning tools to control the session-to-session variability. Consequently, comparing between the EC and Functional Connectivity (FC) is utilized as the generalization capabilities for unseen data in order to classify single resting-state fMRI sessions with respect to healthy subjects. Secondly, both subjects of identity and condition (rest versus movie views) were predicted to verify that EC can disentangle the two types of signatures. Just the Z_axis views were used [**14**]. In 2018, Kazemi *et al*. presented a DL algorithm to classified five different stages of Alzheimer's disease (AD). Network architecture of AlexNet was used to classify different AD stages. The work was successfully classified the Significant Memory Concern (SMC), Early Mild Cognitive Impair (EMCI), AD, Late Cognitive Mild Impair (LMCI) and Normal Healthy Control (NC). Successful performances were attained for each class [**15**]. In 2019, VanRullen *et al*. applied a recently developed DL system to reconstruct face images from the fMRI of individuals. A Variational Auto-Encoder (VAE) neural network was trained by using a Generative Adversarial Network (GAN). Unsupervised procedure was considered over a large number of celebrity faces. The results showed that some advantages of face recognition and gender classification could be taken from the expressive power of deep generative neural networks (in particular the VAEs coupled with the GANs). This leaded to provide better image spaces of decoded brain information. Front parietal, temporal and occipital views were considered [**16**]. In 2019, Al-Zubaidi *et al.* studied the influence of hunger and satiety on resting-state functional Magnetic Resonance Imaging (rs-fMRI). Three connectivity models of the local connectivity, global connectivity and amplitude rs-fMRI signals were investigated. Connectivity parameters of 90 brain regions were extracting for each model. Sequential forward floating selection strategy and linear Support Vector Machine (SVM) classifier were used. It was found that the amplitude of rs-fMRI signals is slightly more precise in local than global connectivity models in detecting brain changes during the hunger and satiety [**17**]. In the same year, Pani *et al.* suggested classifying the resting-state of fMRI features exemplified by the metabolic state of hunger and satiety. The authors utilized Logistic Regression (LR) and SVM methods. Generally, the LR provided better scores compared to the SVM [**18**]. For the literature it can be observed that only several studies considered classifying brain activities based on DL techniques. In addition, classifying patterns of vision, movement and forward activities based on the three views of (X_axis, Y_axis and Z_axis) has not been considered before. Therefore, this study will be presented to overcome the obstacles of these issues.

July-August 2020
ISSN: 0193-4120 Page No. 3035 - 3052

III. THE METHODOLOGYAND MATERIALS

1- Descriptions of the Employed Real Clinical Dataset

The dataset that is used in this work is from the Ethics Committee of Aston University (ECAU) and it basically has real clinical fMRI images. It was collected from 13 subjects or persons, who are native Italian speakers, of ages between 25 – 42 years. Six of them are women. The data was acquired based on using the efMRI. The fMRI is used to facilitate the estimation of the HRF. In this study, the fMRI images were acquired using 8-channels of radiofrequency head coil. Type Siemens medical systems from Germany with a 3 Tesla using Siemens Trio MRI scanner is employed. Functional images were collected using a T2*-weighted Echo Planar Imaging (EPI) sequence, which is sensitive to the BOLD contrast. Each image was captured with the following specifications: Time of Echo (TE) equal to 30 ms, Time of Repetition (TR) equal to 3.0 s, image matrix equal to 64 × 64 pixels, Field of View (FOV) equal to $216 \times 216 \times 129$ mm^3, flip angle equal to 90 degree, voxel size equal to 3 × 3 mm and slice thickness equal to 3 mm. Brain volumes were acquired in a series of slices, where a total number of slices are 44. Between 765 and 800 volumes per participant were collected in a single session.

2- Classification Models

First of all, there are many tasks that are dominated by the brain. Three tasks of vision, motor and prefrontal cortices are focused here for two reasons. The first reason is to cover the tasks that are daily used by a person and are directly affected on his/her life. The second reason is to study the classification of vital brain parts that cover different tasks in most brain lobes. So, starting from the prefrontal cortex for making-decision (anterior part of the brain). Moving on to just near the central sulcus (furrow), the region which separates the frontal lobe from the parietal lobe, for performing the motor activity (middle part of the brain). Ending with the occipital lobe for visual activity (posterior part of the brain).

In this study, a new scheme to classify the brain activities of vision, movement and prefrontal cortices are presented. Three DL networks are designed, combined and implemented to achieve high classification accuracies. Fundamentally, this work is consisted of multiple logical stages. Firstly, the images of vision, movement and prefrontal brain activities are collected and all the orthogonal patterns of (X_axis, Y_axis and Z_axis) are considered and presented as a comprehensive study. Then, image pre-processing steps are performed as all the employed images require kind of normalization such as cropping. In addition, the employed images are divided into two sets for the training phase and testing phase. Consequently, DL models are designed as XCM, YCM and ZCM. Principally, all the network models are trained by utilizing the trained images set and the same networks are tested by using the tested images set. Furthermore, DL parameters of convolution, ReLU and pooling layers are evaluated in terms of obtaining the highest accuracies. Subsequently, fusing or combining the outputs of all the proposed DL models is performed. This can increase the confidence classification decisions by considering the outputs of three axes views (X_axis, Y_axis and Z_axis). Fig. 1 shows the most important stages of this work.

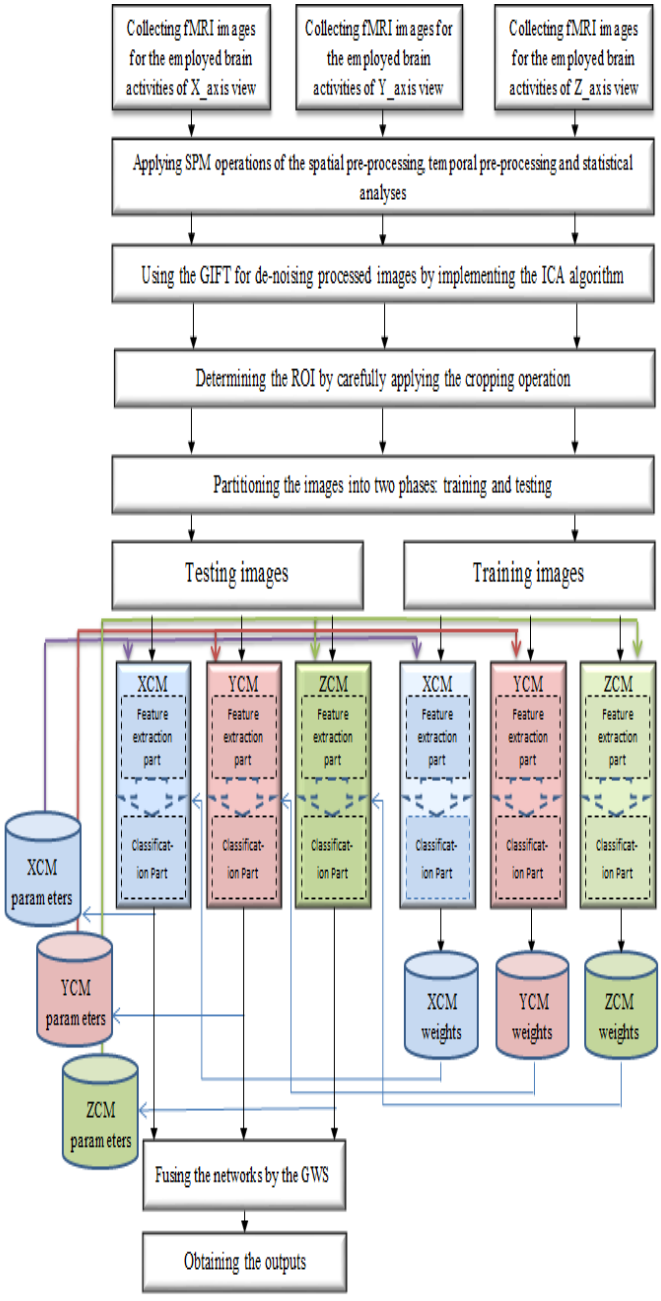

Figure 1: Required processing stages in this study, it shows fully suggested scheme

As mentioned, the three network proposed models are based on the CNN. Each model adapts to accept a specific view of fMRI images, contains evaluated parameters of its multiple layers and efficiently classifies the employed brain activities. The three models have simple yet effective

July-August 2020
ISSN: 0193-4120 Page No. 3035 - 3052

structures. The essential layers of input, convolution, ReLU, pooling, FC, softmax and output layers are exploited . It can be show in Fig. 2. Each layer has different specifications and parameters as will be explained in the next sub-sections.

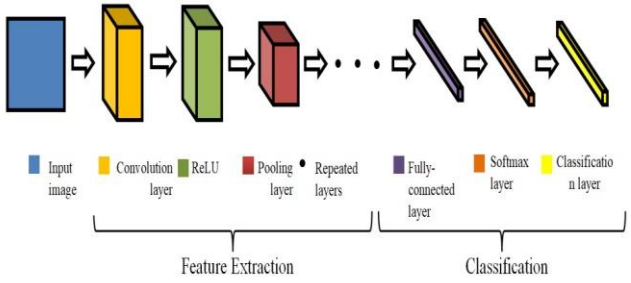

Figure 2: A general CNN architecture for image classification task

Input layer deals with images. It collects values of input matrix pixels depending on the resolution and size of the image. In this study, a Joint Photographic Group (JPG) colored image with the dimensions of (width × height × 3) pixels are used. The 3 refers to three channels of Red, Green and Blue (RGB) that compose the colored image which is known as the RGB image too. Whereas, the width and height are adapted for each proposed model according to the required view of (X-axis, Y-axis and Z-axis). The RGB channels of the input matrix are separately filtered in the next layer (the convolution layer) [**19**].

Convolution layer consists of sets of image channels and kernels. In this layer, each input channel is convolved by kernels. Implementing this operation with different kernels will produce a set of feature maps. Each kernel represents a group of weights [96]. In other word, the kernel values can be considerd as the weight values [**20**]. Channels are convolved by kernels after dividing each channel into small windows. Resulted image channels known as feature maps. The feature map values are calculated according to the following formula [**21**]**:**

$$F_{u,v,c}{}^{l} = U_c{}^{l} + \sum_{i=-H_h^l}^{H_h^l} \sum_{j=-H_w^l}^{H_w^l} \sum_{c^{l-1}=1}^{c^{l-1}} W^{c^l}{}_{i+H_h^l, j, H_w^l, c^{l-1}} F_{u+i,v+j,c^{l-1}} \quad (1)$$

where: $F_{u,v,c}{}^{l}$ is an output of the convolution layer, (u,v) is a pixel coordinate, $U_c{}^{l}$ is the channel bias, $W_{i,j,c^{l-1}}^{c^l}$ is the kernel weighs, c is the channel number, H_w^l and H_h^l are respectively the width and height of the convolution layer kernel, l is the current layer, and $l-1$ is the previously layer.

It has the ability to filter each channel image by fixed kernel values, in other words, weights. Multiple feature maps can be generated by exploiting different kernels for each channel. This can provide various filtering analyses for each channel image. For implementing convolution operations, different parameters of filter size, number of filters, padding and stride can be utilized [**22**].

ReLU is the most commonly used activation function in the DL networks, especially in the CNN models. It works by activating an ANN to pass a positive value or zero. When comparing this with a BNN of brain, the activation function decides whether a neuron is fired or not [**20**]. This layer provides non-linear computation to the CNN. Its function results 0 if it receives any negative value (removes the negative values) whereas; it keeps any positive value (preserves the positive values). It can be expressed as:

$$R_{u,v,c}{}' = \max(0,\ F_{u,v,c}{}') \quad (2)$$

where: $R_{u,v,c}{}'$ is the output of ReLU, max is the maximum operation and $F_{u,v,c}{}'$ is an input positive value to the ReLU activation function [**22**].

Pooling is down-sampling information. This layer can further reduce the spatial dimensions, but not depth. It is added after the convolution operations, specifically, after the nonlinearity of ReLU. It operates with each feature map separately and creates a new set of feature maps [**23**]. The size of a pooling operation must be smaller than the size of a feature map. This leads to reduce the number of pixels in each previous feature map as shown in Fig 4.3. So, pooling layer can help in decreasing the size of feature maps and increasing the performance by reducing the over fitting [**24**] of the model. Two common pooling types are:

- **Maximum Pooling (MP):** it calculates the maximum values of small matrices (windows) in each previous feature map. The MP operation is applied according to the following equation [**25**]:

$$T_{a^l,b^l,c\,Max} = \underset{0 \le a < ph, 0 \le b < p_w}{\text{MAX}} R_{a^l \times ph + a, b^l \times p_w + b, c} \quad (3)$$

where: $T_{a^l,b^l,c\,Max}$ is an output of the pooling layer of maximum type , $0 \le al < phl$, phl is the height of the pooled channel, $0 \le bl < pwl$, pw is the width the pooled channel, $0 \le c < cl = cl\text{-}1$, ph is the height of each pooled window and pw is the width of each pooled window.

- **Average Pooling (AP):** it calculates the average values of small matrices (windows) in each previous feature map. The AP operation is applied according to the following equation [**26**]:

$$f_{ave}(R) = \frac{1}{S \times S} \sum_{i=1}^{S} R_i \quad (4)$$

where: f_{ave} is an output of the pooling layer of average type, S is the pooling region size and R_i is the output ReLU.

The FC layer connects each node from a previous layer to all node of this layer. It can adapt between the number of nodes in the feature extraction part and the number of nodes in the classification part of a DL model. It turns feature maps into a vector and it is the first layer in classification

July-August 2020
ISSN: 0193-4120 Page No. 3035 - 3052

part [**25**]. The output of this layer will be composed according to the following equation:

$$P_r = \sum_{a=1}^{n_1^{l-1}} \sum_{b=1}^{n_2^{l-1}} \sum_{c=1}^{n_3^{l-1}} U_{a,b,c,r}^{l} (T_s)_{a,b} \qquad \forall 1 \le r \le n' \qquad (5)$$

where: P_r is an output of the FC layer, n_1^{l-1} is the previous pooling channel width, n_2^{l-1} is the previous pooling channel height, n_3^{l-1} is the number of previous pooling channels, $(T_s)_{a,b}$ is a pooling layer output, $U_{a,b,c,r}^{l}$ is a weight between the pooling and FC layers and n' is the required number of classes.

The softmax layer is normally applied just before the last layer, which is the classification layer. The reason of using the softmax is to provide the relating probability distributions with all output classes for a current input. However, it may become costly if the number of classes is further increased [**20**]. Mathematically, the softmax function is shown as given in the following equation:

$$y_r = \frac{exp(P_r)}{\sum_{s=1}^{n^{l-1}} exp(P_s)} \qquad (6)$$

where: y_r is an output of the softmax layer.

In other words, the softmax function normalizes the output values of each single node to be between 0 and 1. It divides the value of each output by the total summation of other output values.

The classification layer is the last layer. It classifies a provided input to its closest class. It produces the output decision. This layer operates according to the rule called the winner-takes-all [**27**]. The operation of this layer can be described as follows:

$$D_r = \begin{cases} 1 & if\ y_r = max \\ 0 & otherwise \end{cases} \qquad (7)$$

where: D_r is an output decision of the classification layer and *max* represents the extracted maximum y_r value.

This last layer has been adapted to classify between the motor, vision and pre-frontal brain parts depending on the location of activity. This is applied to all models of XCM, YCM and ZCM. This trend indicates that this study can reasonably succeeded in providing valuable recognition of various employed brain activities for each axis.

IV. SUGGESTED FUSION METHOD

A single classifier was always used in a traditional pattern recognition system. In recent years, it has been found that the samples that gives less accuracy in a distinct classifier can be enhanced by using a fusion method. Multiple classifier systems can usually obtain higher classification accuracies compared with a single classifier [28]. Currently, multiple classifier fusion method have been adopted in many applications such as medical diagnosis [29], fault diagnosis [30] [31], remote sensing [32] [33], face recognition [34], intrusion detection [35] and finger recognition [20]. Some of the fusion methods have good generality and can show good classification performances. However, there is no fusion method that can obtain the optimal classification performance for all applications. In this work, the decision fusion is effectively employed and found to attain high performances. In this study and as mentioned three models XCM, YCM and ZCM are suggested, fusion decision is able to provide high performances by combining all of the suggested models. Final decisions are performed based on the widely provided outcomes from the three proposed models.

A GWS rule is suggested here to find the optimal values of weights, which are exploited to fuse between the proposed DL models (the XCM,YCM and ZCM). It is based on the Genetic Algorithm (GA). The GA is an optimization algorithm that uses the strategies of natural real genetic manners. That is, it is the process of transferring genetic traits from parents to offspring by sharing between their chromosomes. The evolution is iteratively processed. The information are passed from parents to offspring according to cell divisions and fertilizations to create new offspring at each generation. During genetic generation may happens genetic variations can arise from gene mutations. it is a normal process in which genetic material is rearranged as a cell is getting ready to divide by add and remove chromosomes.

First of all, a set of random values (or chromosomes) are selected and used for the processing, it is called "population". The number of chromosomes in a population is termed the "population size" and the total number of genes (values) in each chromosome is named the "string length". The population in each iteration is known as "generation". In each generation, a "fitness function" is evaluated for each individual population. The fitness function is the evaluation equation that requires to be optimized. It is the most important equation in the GA and it is assessed by using the GA chromosomes. Population genes are processed by applying various operations of "crossover", "mutation" and "selection" [36]. The crossover it is a genetic operator used to combine the genes information for two parents of chromosome to generate new offspring chromosomes. This operation is implemented with the most generations. The mutation is also a genetic operator utilized to change a gene value in a chromosome. This operation is executed with a less number of generations. The selection is the method of choosing chromosomes to be parents after evaluating with the fitness function.

A new generation of chromosomes is iteratively produced and examined. This process is carried out until the optimal solution is reached by the most appropriate chromosome(s) [37]. The GA has the ability to avoid being trapped by local minima or local maxima as traditional methods.

The evolution process in the GA starts with the creation of the initial population. Usually, the population chromosomes are encoded by bit strings of '1' or '0' values. When the first population is created, the fitness function is evaluated. Then, the selection operation identifies the fittest candidates to breed. A crossover operation works with a couple of selected chromosomes (parents) by exchanging their

July-August 2020
ISSN: 0193-4120 Page No. 3035 - 3052

substrings, where a double of offspring (children) is generated [38]. A mutation operation changes a value of a randomly selected gene in the offspring as changing between '0' and '1'. In each generation, a portion of existing population is selected to breed a new offspring. The fitness function is always assessed for how close a chromosome to the optimal solution. The optimal solution can be a maximum global or minimum global value. At the end, the chromosome(s) that can report the best fitness function value is(are) recorded.

In this study, minimizing the total error value of classifying the employed brain activities is considered by applying the following fitness function:

$$\varepsilon = \frac{\sum_{i=1}^{n} |(\psi_1 Y1_i + \psi_2 Y2_i + \psi_3 Y3_i) - V_i|}{n} \quad (8)$$

where: ε is the error value between the fused outputs and targets, ψ_1 is the first weight coefficient of the GWS, $Y1_i$ is the output class number of the XCM, ψ_2 is the seconde weight coefficient of the GWS, $Y2_i$ is the output class number of the YCM, ψ_3 is the third weight coefficient of the GWS, $Y3_i$ is the output class number of the ZCM.

In this study, the GWS was adopted to raise the accuracy by adopting the weight coefficients that are resulting from the GA search. Fig. 3 shows the procedure to find the best weight coefficients of the GWS. The GA is used to optimize the fusion process by producing appropriate weight coefficients. Also, the GA has significant guessing values and it well avoids being trapped by the local minima solution. Table 1 shows the GA parameters that are utilized in this work.

Table 1: The utilized GA parameters in this work

GA parameters	Type/value
Population size	50
Selection function	Roulette
Mutation rate	0.01
Crossover function	Scattered
Crossover fraction	0.8
Stopping criteria (stall generation)	1000

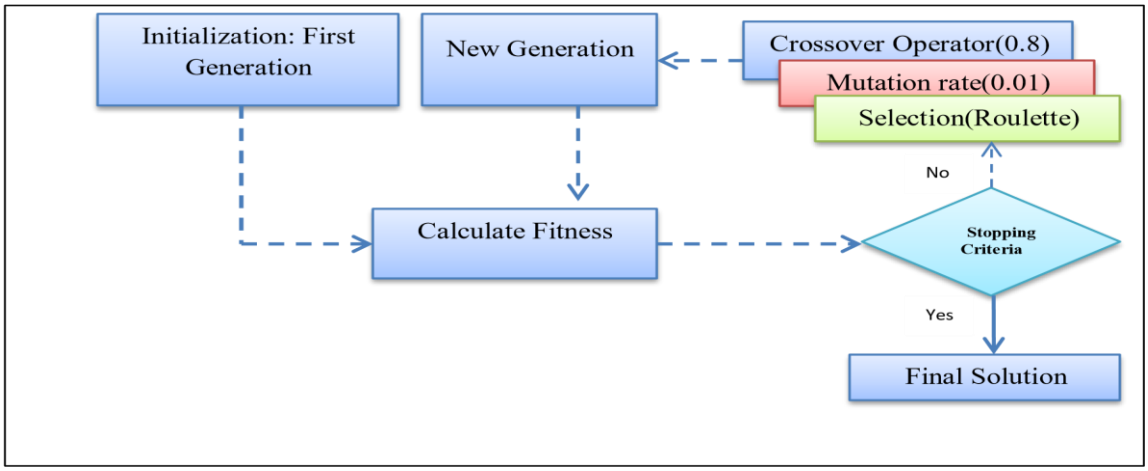

Figure 3: The procedure of determining the optimal weight coefficients of the suggested GWS by the GA

July-August 2020
ISSN: 0193-4120 Page No. 3035 - 3052

V. RESULT AND DISCUSSIONS

1- Analyzing the Real Clinical Dataset

For analyzing of the real clinical dataset, two different Matlab toolboxes are exploited namely the SPM and GIFT. The fMRI data were pre-processed using SPM12 (Wellcome Department of Imaging Neuroscience, London; http://www.fil.ion.ucl.ac.uk) and analysed by Group ICA of fMRI Toolbox (GIFT - http://trendscenter.org/software/gift/). Three views of X-axis, Y-axis and Z-axis are available for the three brain activities of vision, movement and pre-front. In this work, total of 201 images which contain all the views of the three employed brain activities are extracted from 67 fMRI slices. Each slice is of size 654 × 654 × 3 pixels, it is of Joint Photographic Experts Group (JPEG) format and it has a group of colored images. This data is for 13 subjects following [**39**] [**40**] as to the best of the obtained knowledge full of required information are only available for those participants. Samples of brain activity slices are given in Fig. 4.

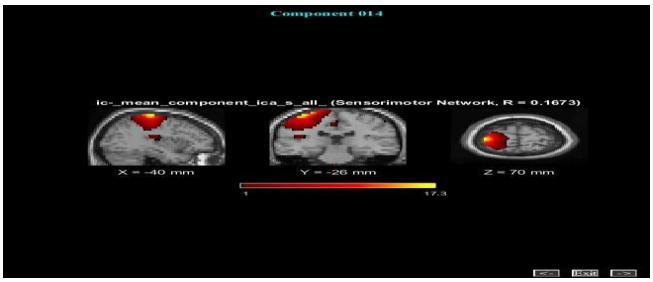

(a)

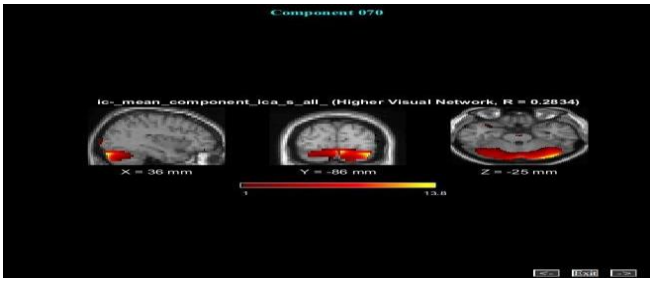

(b)

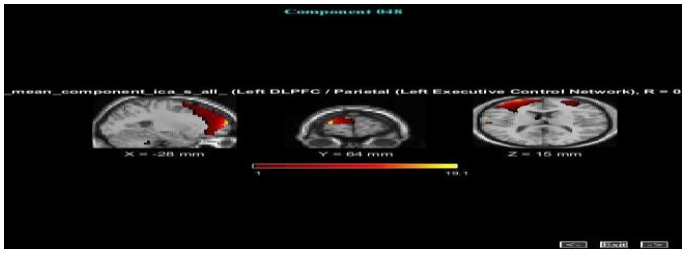

(c)

Figure 4: Samples of fMRI slices for the brain activities of (a) motor/movement, (b) vision and (c) prefrontal. Each activity has been demonstrated from the left to the right with the views of X-axis, Y-axis and Z-axis, respectively

2- Image pre-processing for Deep Learning Networks

Preparing images that are obtained after previous processing is required. The applied pre-processing preparation before the DL classification is the image cropping. Image cropping is utilized to remove undesired information and extract a Region of Interest (ROI) from an image. After the pre-processing, specific sizes are empirically defined for the three viewers of X, Y and Z axes. That is, a size of 147 × 170 × 3 pixels is determined for the X-axis view, a size of 147 × 140 × 3 pixels is assigned for the Yaxis view and a size of 147 × 155 × 3 pixels is specified for the Z- axis view. Moreover, the extracted images are grouped into two phases: training and testing. In this work, all images of the employed brain activities are grouped into 50% for the training phase and 50% for the testing phase. Samples of carefully extracted images after the pre-processing of cropping are given in Fig. 5.

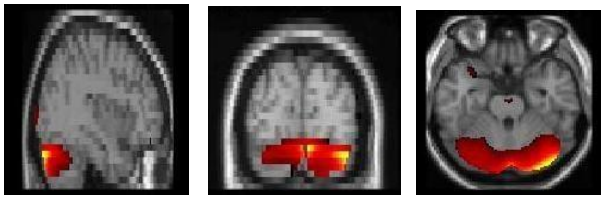

(a)

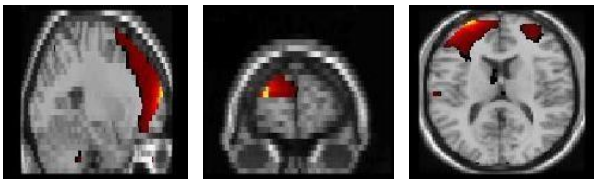

(b)

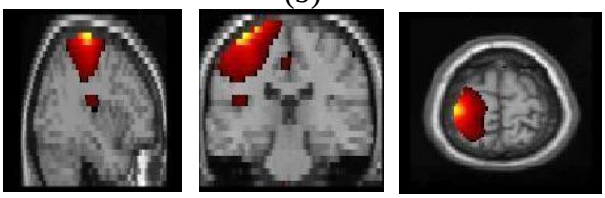

(c)

Figure 5: Samples of carefully extracted images after the cropping for the brain activities of (a) motor/movement, (b) vision and (c) prefrontal, respectively. Each activity has been demonstrated from the left to the right with the views of X-axis, Yaxis and Z-axis, respectively

3- Classification of the Real Clinical Data

Classification is a regular arrangement in a group or category based on recognized feature extraction. Guiding an input to its closest class is performed by producing an output decision of classification. Firstly, DL networks namely the XCM, YCM and ZCM are trained by using the trained groups of images. Secondly, the trained networks are tested by utilizing the

July-August 2020
ISSN: 0193-4120 Page No. 3035 - 3052

tested groups of images. The accuracies of each DL network are assessed by examining the parameters of its layers. Again, classifying brain activity images into vision, motor or pre-front cortex is considered for each view of X-axis, Y-axis and Z-axis.
The suggested XCM, YCM and ZCM networks are designed, trained and tested by using a computer that has the following specifications: laptop of type Dell, Central Processing Unit (CPU) of type Intel Core (TM) i7, 3 GHz and Random-Access Memory (RAM) of 8 GB. All implementations are carried out based on the CPU.
In summary, the proposed DL networks can be signified with other artificial intelligence models as in [41-50]. They can be utilized for important matters as [51-58].

❖ X-axis Classification Model

In the proposed XCM, every layer acts as a detection to classify an employed brain activity by exploiting the X_axis view (sagittal plane) of an fMRI image. Main XCM layers which contain the important parameters that may influence the results are the convolution and pooling layers. For the convolution layer, the parameters of filter/kernel size, number of filters, stride and padding are examined for different values. For the pooling layer, the parameters of type, window size, stride and padding are assessed for various values. Table 2 show the XCM testing performances of tuning or changing the considered parameters (after 100 training epochs). To achieve the highest efficient performance of the suggested XCM network, the parameters are tuned by considering eight cases. Each of these cases involves examining one parameter while leaving the other parameters fixed. Then, the best resulted accuracy is considered and its parameters' values are benchmarked for assessing another parameter. This procedure is used for checking all considered parameters. For the first case, it can be observed from the beginning of Table 2 that when changing the filter size from 3×3 pixels to 13×13 pixels, the best accuracy is recorded for 5 × 5 pixels as it achieved 86.11% after evaluating the XCM network. It has been cited that this size can well analyze image features and overcome the effects of noise [96]. As mentioned, this value is considered for assessing the second parameter of the convolution layer. In the second case, the number of filters is tested, where the number of filters is tuned from 2 to 14 filters. It can be noticed that the best number of filters is 2 where the highest accuracy of 86.11% is recorded. This means that the XCM network does not require many filters to discover the stimulating areas of brain activities. Also, this reduces the consuming time of training and testing this model. The third case involves examining the stride of filters in the convolution layer, where its values are changed from 5 pixels to 1 pixel (vertically and horizontally). This evaluation showed no enhancement in the accuracy. Case four focuses on changing the padding process in the convolution layer. Padding refers to the pixels that can be added to the boundary of resulted feature maps in order to complete their sizes during the convolution operations, which applied for specific sizes of input channel and kernel. It can have a value of 1, 2, … or Same (S) pixels. That is, any integer number represents a boundary size of pixels with zero values and S represents an automatically calculated boundary size of pixels with copying the same last values. It can be seen that any padding value except 1 pixels is negatively affected the performances by reducing the percentages of accuracies. Case five is for altering between the Maximum (Max) and Average (Ave) types of the pooling layer. It can be observed that the accuracy is decreased to 77.78% by applying the Ave type. So, the Max type is benchmarked here as it reported the highest value of 86.11%. This is due to the ability of the Max pooling, where it can extract the highest features that are important to select the activation area in a brain image. On the other hand, the Ave type takes all values into account and computes the mean which may or may not be significant for detecting brain activities. In case six, changing the pooling filter size is examined. The accuracies are evaluated by applying different window sizes, starting from 3 × 3 pixels to 13 × 13 pixels. It can be investigated that the best result of 91.67 % is obtained for 7 × 7 pixels. It appears that this pooling window size is suitable for decreasing the previous dimensionality of feature maps and preserving the patterns of employed activation areas. Case seven includes adjusting the stride of pooling from 1 pixel to 7 pixels (horizontally and vertically). This process can define the number of overlapped pixels between the pooling windows in a feature map. The best percentage has been recorded for the 3 pixels. This value of stride provides appropriate overlaps between the instances of features. Case eight deals with testing the padding values of 0, 1, 2, 3, 4 and S pixels. Best accuracy is reported for the padding value of 1 pixels, which can be considered as the appropriate tuning parameter here. Adding more padding values increases the total width of a feature map and this often includes undesirable information. Thus, this may decrease the performances of the XCM.
At the end of the applied experiments, the parameters that have resulted with the highest accuracy are: 5 × 5 pixels for the convolution filter size, 2 convolution filters, 1 stride pixel for the convolution kernel, 1 padding pixels for the convolution and pooling layers, Max pooling type, 3 × 3 pixels for the size of pooling window and 3 stride pixels for the pooling windows.
It is worth mentioning that adding more layers of convolution, ReLU and pooling are also explored for the XCM. By implementing two sequential convolution and ReLU layers, the result decreased to 77.78%. Furthermore, by applying three sequential convolution, ReLU and max-pooling layers, the accuracy further decreased to 36.11%. These performances are obviously less than the best benchmarked percentage. Therefore, their parameters have been discarded.
To conclude the main findings in the XCM, the X_axis view for the fMRI images is preferable in classification investigations of brain activities. This is because of the clarity of provided information.

July-August 2020
ISSN: 0193-4120 Page No. 3035 - 3052

Table 2 : Extensive experiments to examine the accuracies of tuning various XCM parameters

Cases	Parameters of the convolution layer				Parameters of the pooling layer				Accuracy (%)
	Filter size	No. of filters	Stride	Padding	Type	Window size	Stride	Padding	
1	3×3	2	1	1	Max	3×3	3	1	83.33
	5×5	2	1	1	Max	3×3	3	1	86.11
	7×7	2	1	1	Max	3×3	3	1	66.67
	9×9	2	1	1	Max	3×3	3	1	72.22
	11×11	2	1	1	Max	3×3	3	1	66.67
	13×13	2	1	1	Max	3×3	3	1	72.22
2	5×5	2	1	1	Max	3×3	3	1	86.11
	5×5	4	1	1	Max	3×3	3	1	75
	5×5	6	1	1	Max	3×3	3	1	80.56
	5×5	8	1	1	Max	3×3	3	1	75
	5×5	10	1	1	Max	3×3	3	1	80.56
	5×5	12	1	1	Max	3×3	3	1	72.22
	5×5	14	1	1	Max	3×3	3	1	75
3	5×5	2	5	1	Max	3×3	3	1	83.33
	5×5	2	4	1	Max	3×3	3	1	83.33
	5×5	2	3	1	Max	3×3	3	1	80.55
	5×5	2	2	1	Max	3×3	3	1	77.78
	5×5	2	1	1	Max	3×3	3	1	86.11
4	5×5	2	1	0	Max	3×3	3	1	75
	5×5	2	1	1	Max	3×3	3	1	86.11
	5×5	2	1	2	Max	3×3	3	1	83.33
	5×5	2	1	3	Max	3×3	3	1	72.22
	5×5	2	1	4	Max	3×3	3	1	83.33
	5×5	2	1	S	Max	3×3	3	1	83.33
5	5×5	2	1	1	Max	3×3	3	1	86.11
	5×5	2	1	1	Ave	3×3	3	1	77.78
6	5×5	2	1	1	Max	3×3	3	1	86.11
	5×5	2	1	1	Max	5×5	3	1	75
	5×5	2	1	1	Max	7×7	3	1	91.67
	5×5	2	1	1	Max	9×9	3	1	88.89
	5×5	2	1	1	Max	11×11	3	1	83.33
	5×5	2	1	1	Max	13×13	3	1	80.56
7	5×5	2	1	1	Max	7×7	7	1	80.56
	5×5	2	1	1	Max	7×7	6	1	83.33
	5×5	2	1	1	Max	7×7	5	1	75
	5×5	2	1	1	Max	7×7	4	1	77.78
	5×5	2	1	1	Max	7×7	3	1	91.67
	5×5	2	1	1	Max	7×7	2	1	86.11
	5×5	2	1	1	Max	7×7	1	1	83.33
8	5×5	2	1	1	Max	7×7	3	0	80.56
	5×5	2	1	1	Max	7×7	3	1	91.67
	5×5	2	1	1	Max	7×7	3	2	55.56
	5×5	2	1	1	Max	7×7	3	3	83.33
	5×5	2	1	1	Max	7×7	3	4	86.11
	5×5	2	1	1	Max	7×7	3	S	80.56

July-August 2020
ISSN: 0193-4120 Page No. 3035 - 3052

❖ Y-axis Classification Model

The YCM is suggested for the classification of employed brain activities, but by using the Y_axis view (coronal plane) of fMRI images. It also consists of essential multiple layers. These are the convolution, ReLU, pooling, FC, softmax and classification layers. Likewise the XCM procedure (in previous sub-section), similar processes are applied for the YCM. Table 3 show the YCM testing accuracies of changing the considered parameters (after 100 training epochs).

From Table 3, the first case of examining YCM parameters is for changing the filter size of the convolution layer from 3×3 pixels to 13×13 pixels with settling all the values of other parameters. Best accuracy of 80.56% is recorded for the 3 × 3 pixels and 11 x 11 pixels as these kernel sizes can improve the activation patterns detection. In this matter and because the same accuracy is obtained, the consuming time is worth to be considered. That is, the network consumes more training time with the window size of 11 × 11 pixels than the 3 × 3 pixels. So, the 3 × 3 pixels are selected. This value is assigned for evaluating the second parameter of the convolution layer. In the second case, the second parameter to be assessed is the number of filters. It is varied from 2 to 14 filters. It can be observed that the best number of filters is 14 where the accuracy of 83.33% is reported. This means the YCM network consumes a big number of filters to discover the activation area of the employed brain activities. The third case includes checking the stride in the convolution layer by testing the three values of 3, 2 and 1 pixels. Stride 2 pixels increases the accuracy to 86.11% as this value can provide suitable overlap between the information of applied channels. Tuning this value by using a big or small number leads to decrease the overall performance. Case four involves testing the padding of the convolution layer by changing its values between 0, 1, 2, 3, 4 and S pixels. It can be investigated that all the values except 1 in this evaluation are negatively affected the accuracies. In addition, for the values 3 and 4, out of memory problems are noticed. Case five concentrates on altering between the main pooling types (Max/Ave) in the pooling layer. The accuracy is fixed here to 86.11% in both cases. This caused doing more extensive evaluations in order to reasonably decide which type can be selected. In case six, the pooled window size is tuned from 3 × 3 to 13 × 13 pixels for both pooling types. It can be seen that the best result of 88.89% is given for the 11 × 11 pixels with the Max type. The Max pooling type proves its efficiency again in the YCM. This is consistent with the selection type of the XCM. Regarding the pooling window size of 11 × 11 pixels, it allows further reduction for the previous dimensionalities and preserves the characteristics of applied activation areas.

Case seven includes tuning the stride values of the pooling layer from 4 to 11. It can be noticed that the accuracies attained the highest result of 88.89% in the strides 6 and 7 pixels. The stride 7 pixels are assigned because large stride causes small overlaps, which means getting decreased output sizes. In addition to other advantages as reducing the required memory, simplifying the DL processing and avoiding the over fitting. Case eight deals with testing the pooling layer padding for the values 0, 1, 2, 3, 4 and S pixels. The same suitable padding value of 1 pixels for the XCM is obtained here for the YCM. Again, including more padding pixels negatively influences the performance as they lead to increase the width of a channel by adding undesired information. Also, the additional information cause applying more calculations. At the end of implemented experiments, the parameters that have produced the highest performance for the convolution layer are: filter size of 3 × 3 pixels, number of filters equal to 14 filters, stride of 2 pixels and padding of 1 pixels, and for the pooling layer are: Max type, window size of 11 × 11 pixels, stride of 7 pixels and padding of 1 pixels too.

Adding more layers of convolution, ReLU and pooling are also discovered for the YCM. By applying two sequential convolution and ReLU layers, the accuracy again decreased to 77.78%. Furthermore, by implementing three sequential convolution, ReLU and max-pooling layers, the result dropped to 33.33%. These performances are clearly less than the best recorded percentage. Thus, their parameters have been ignored.

To sum up the main findings in the YCM, the Y_axis view for the fMRI images can be considered as a challenging perspective to detect brain activities. This is due to the provided narrow information for the closest brain parts in the images.

Table 3 : Extensive experiments to examine the accuracies of tuning various YCM parameters

Cases	Parameters of the convolution layer				Parameters of the pooling layer				Accuracy (%)
	Filter size	No. of filters	Stride	Padding	Type	Window size	Stride	Padding	
1	3×3	2	1	1	Max	3×3	3	1	80.56
	5×5	2	1	1	Max	3×3	3	1	75
	7×7	2	1	1	Max	3×3	3	1	77.78
	9×9	2	1	1	Max	3×3	3	1	72.78
	11×11	2	1	1	Max	3×3	3	1	80.56
	13×13	2	1	1	Max	3×3	3	1	75
2	3×3	2	1	1	Max	3×3	3	1	80.56
	3×3	4	1	1	Max	3×3	3	1	80.56
	3×3	6	1	1	Max	3×3	3	1	80.56
	3×3	8	1	1	Max	3×3	3	1	80.56
	3×3	10	1	1	Max	3×3	3	1	77.76
	3×3	12	1	1	Max	3×3	3	1	80.56
	3×3	14	1	1	Max	3×3	3	1	83.33
3	3×3	14	3	1	Max	3×3	3	1	83.33
	3×3	14	2	1	Max	3×3	3	1	86.11
	3×3	14	1	1	Max	3×3	3	1	83.33
4	3×3	14	2	0	Max	3×3	3	1	69
	3×3	14	2	1	Max	3×3	3	1	86.11
	3×3	14	2	2	Max	3×3	3	1	83.33
	3×3	14	2	3	Max	3×3	3	1	N/A[(1)]
	3×3	14	2	4	Max	3×3	3	1	N/A
	3×3	14	2	S	Max	3×3	3	1	83.33
5	3×3	14	2	1	Max	3×3	3	1	86.11
	3×3	14	2	1	Ave	3×3	3	1	86.11
6	3×3	14	2	1	Max	3×3	3	1	86.11
	3×3	14	2	1	Max	5×5	3	1	80.56
	3×3	14	2	1	Max	7×7	3	1	77.76
	3×3	14	2	1	Max	9×9	3	1	86.11
	3×3	14	2	1	Max	11×11	3	1	88.89
	3×3	14	2	1	Max	13×13	3	1	86.11
	3×3	14	2	1	Ave	3×3	3	1	86.11
	3×3	14	2	1	Ave	5×5	3	1	69.44
	3×3	14	2	1	Ave	7×7	3	1	72.22
	3×3	14	2	1	Ave	9×9	3	1	83.33
	3×3	14	2	1	Ave	11×11	3	1	77.78
	3×3	14	2	1	Ave	13×13	3	1	69.44
7	3×3	14	2	1	Max	11×11	11	1	77.76
	3×3	14	2	1	Max	11×11	10	1	86.11
	3×3	14	2	1	Max	11×11	9	1	83.33
	3×3	14	2	1	Max	11×11	8	1	83.33
	3×3	14	2	1	Max	11×11	7	1	88.89
	3×3	14	2	1	Max	11×11	6	1	88.89
	3×3	14	2	1	Max	11×11	5	1	86.11
	3×3	14	2	1	Max	11×11	4	1	83
	3×3	14	2	1	Max	11×11	7	0	80.11
	3×3	14	2	1	Max	11×11	7	1	88.89

(1) N/A means problem.

July-August 2020
ISSN: 0193-4120 Page No. 3035 - 3052

❖ Z-axis Classification Model

The ZCM is proposed for classifying the employed brain activities by utilizing the Z_axis view (axial plane) of fMRI images. Again, similar procedure that is used for the XCM and YCM (in previous two sub-sections) is exploited here for the ZCM. Table 4 show the ZCM testing results of tuning the considered parameters (after 100 training epochs).

For the first case, it can be observed from the beginning of Table 4 that the filter size parameter of the convolution layer is examined for the values from 3 × 3 pixels to 13 × 13 pixels. The best accuracy is reported for the 3 × 3, 5 × 5, 9 × 9 and 11 × 11 pixels where they all attained the same value of 86.11%. As previously mentioned, it is worth to choose the filter size according to the consuming time of training. Thus, the window filter size of 3 × 3 pixels is assigned. It has been cited that this size can detect the micro textures of image [59]. As mentioned, this value is benchmarked and used for evaluating the second parameter. In the second case, the number of filters of the convolution layer is checked where this parameter is tuned from 2 to 14 filters. It can be noticed that the best number of filters is 2 as the accuracy here is obtained equal to 86.11%. This means that the ZCM network does not require many filters and it consumes less time for training and testing. The third case involves examining the stride in the convolution layer where its values are changed from 1 to 3 pixels. However, this evaluation showed that the accuracy does not enhance for 2 and 3 pixels, in fact it is decreased. Case four focuses on changing the padding values in the convolution layer. The padding is assessed for the values of 0, 1, 2, 3, 4, 5 and S pixels. Likewise the XCM and YCM, the best appropriate padding value is benchmarked for 1 pixels. As mentioned, adding more padding values increases the sizes of channels by generating more undesired values. This requires more calculations and decreases the performances of the ZCM. Case five is utilized for altering between the Max and Ave types of the pooling layer. It can be seen that the accuracy is decreased to 80.56% when applying the Ave type. Therefore, the Max type is chosen, because it attained the highest percentage of 86.11%. Again, this type can extract the most important features of the employed brain activities. Whereas, the Ave type considers the mean values of features. In case six, changing the pooled window size is examined for the values from 3 × 3 pixels to 13 × 13 pixels. Then, the best percentage is given for 9 × 9 pixels where the accuracy is raised to 91.67%.. Case seven includes adjusting the stride of pooling for the values from 2 to 9 pixels. It can be seen that the network accuracies attained the best impact with the value of 3 pixels. Case eight provides testing the padding values of the pooling layer where six tuned values of 0, 1, 2, 3, 4 and S pixels are investigated. The best performance is again reported for the padding value of 1 pixels. This is the same obtained value in the convolution layer and its same explanation can be considered here. At the end of operated experiments, the parameter values that have achieved the highest accuracy for the convolution layer are: filter size equal to 3 × 3 pixels, number of filters equal to 2, stride equal to 1 pixels and padding equal to 1 pixels. Furthermore, the best parameter values for the pooling layer are: Max type, window size equal to 9 × 9 pixels, stride equal to 3 pixels and padding equal to 1 pixels.

Also, adding more layers of convolution, ReLU and pooling are investigated for the ZCM. By executing two sequential convolution and ReLU layers, the accuracy reduced to 72.22%. Furthermore, by implementing three sequential convolution, ReLU and max-pooling layers, the percentage significantly decreased to 30.56%. These results are obviously less than the best achieved performance. So, their parameters have been neglected.

To summarize the major findings in the ZCM, the Z_axis view for the fMRI images is also preferable in classification studies of brain activities. In fact, the Z_axis is the most popular view and it can be considered as the optimal visualization because of the useful clarity in its provided information.

July-August 2020
ISSN: 0193-4120 Page No. 3035 - 3052

Table 4 : Extensive experiments to examine the accuracies of tuning various ZCM parameters

Cases	Parameters of the convolution layer				Parameters of the pooling layer				Accuracy (%)
	Filter size	No. of filters	Stride	Padding	Type	Window size	Stride	Padding	
1	3×3	2	1	1	Max	3×3	3	1	86.11
	5×5	2	1	1	Max	3×3	3	1	86.11
	7×7	2	1	1	Max	3×3	3	1	72.22
	9×9	2	1	1	Max	3×3	3	1	86.11
	11×11	2	1	1	Max	3×3	3	1	86.11
	13×13	2	1	1	Max	3×3	3	1	75
2	3×3	2	1	1	Max	3×3	3	1	86.11
	3×3	4	1	1	Max	3×3	3	1	75
	3×3	6	1	1	Max	3×3	3	1	66.67
	3×3	8	1	1	Max	3×3	3	1	83.33
	3×3	10	1	1	Max	3×3	3	1	75
	3×3	12	1	1	Max	3×3	3	1	83.33
	3×3	14	1	1	Max	3×3	3	1	69.44
3	3×3	2	3	1	Max	3×3	3	1	80.56
	3×3	2	2	1	Max	3×3	3	1	83.33
	3×3	2	1	1	Max	3×3	3	1	86.11
4	3×3	2	1	0	Max	3×3	3	1	83.33
	3×3	2	1	1	Max	3×3	3	1	86.11
	3×3	2	1	2	Max	3×3	3	1	83.33
	3×3	2	1	3	Max	3×3	3	1	N/A
	3×3	2	1	4	Max	3×3	3	1	N/A
	3×3	2	1	S	Max	3×3	3	1	83.33
5	3×3	2	1	1	Max	3×3	3	1	86.11
	3×3	2	1	1	Ave	3×3	3	1	80.56
6	3×3	2	1	1	Max	3×3	3	1	86.11
	3×3	2	1	1	Max	5×5	3	1	77.78
	3×3	2	1	1	Max	7×7	3	1	77.78
	3×3	2	1	1	Max	9×9	3	1	91.67
	3×3	2	1	1	Max	11×11	3	1	86.11
	3×3	2	1	1	Max	13×13	3	1	83.33
7	3×3	2	1	1	Max	9×9	9	1	88.89
	3×3	2	1	1	Max	9×9	8	1	83.33
	3×3	2	1	1	Max	9×9	7	1	88.89
	3×3	2	1	1	Max	9×9	6	1	69.99
	3×3	2	1	1	Max	9×9	5	1	75
	3×3	2	1	1	Max	9×9	4	1	83.33
	3×3	2	1	1	Max	9×9	3	1	91.67
	3×3	2	1	1	Max	9×9	2	1	75
8	3×3	2	1	1	Max	9×9	3	0	83.33
	3×3	2	1	1	Max	9×9	3	1	91.67
	3×3	2	1	1	Max	9×9	3	2	86.11
	3×3	2	1	1	Max	9×9	3	3	86.11
	3×3	2	1	1	Max	9×9	3	4	86.11
	3×3	2	1	1	Max	9×9	3	S	86.11

July-August 2020
ISSN: 0193-4120 Page No. 3035 - 3052

❖ Fusion Decision

In this study, the decision fusion can play an important role in improving the results of the XCM, YCM and ZCM. It is able to achieve high performances. As mentioned, there are various rules which can be employed to perform the fusion design such as the minimum, maximum, average, voting rules and weighted-summation. These fusion rules with the suggested GWS have different impacts to overall classification performance. Table 5 shows comparisons between the accuracies of the various fusion rules.

Table 5: Comparisons between the accuracies of the various fusion rules

Rule	Parameter(s)	Accuracy (%)
Minimum rule	_____	86.11
Maximum rule	_____	94.44
Average rule	_____	91.67
Voting rule	MV $\geq$ 2	91.67
Weighted-summation rule	$\omega_1 = 0.5$ $\omega_2 = 0.2$ $\omega_3 = 0.3$	94.44
Suggested GWS rule	$\psi_1 \cong 0.27$ $\psi_2 \cong 0.51$ $\psi_3 \cong 0.36$	97.22

After applying the different fusion rules between the multiple views of brain activities (the X_axis, Y_axis and Z_axis), it can be observed that the minimum fusion rule has negative effect on the overall model. It achieved the inferior accuracy percentage of 86.11%. This is due to considering only the minimum values of the outputs and ignore other values. The average and voting rules recorded a performance of 91.67%. This percentage is reasonably increased because these rules are more concentrated on only the highest values. The maximum and weighted-summation rules both attained the accuracy value of 94.44%. The maximum rule considers the maximum posterior values. It appears that the fusion confidence here is low, because the other outputs are entirely discarded. The weighted-summation rule obtained a high performance according to its selected weight coefficients. What has been reported in the table is for the best achieved accuracy. This rule considers all the output values but with different weights. Obviously, the suggested GWS rule proves it successfulness by raising the accuracy to 97.22%. See Fig. 6. The advantage of the GWS over other optimization techniques is that it has the ability to extract the best fusion values of weight coefficients.

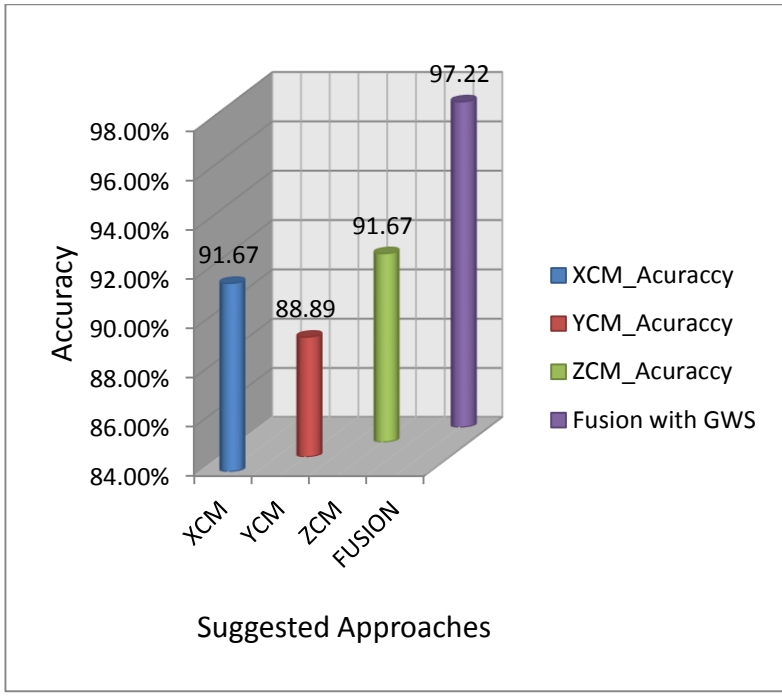

Figure 6: The performances of XCM, YCM and ZCM, and their fusion by the GWS

By this rule, chromosomes are processed in each generation to produce offsprings of next populations. Many offsprings are generated and evaluated until the weight coefficients that minimize the employed fitness function can reach the best result. Fig. 7 demonstrates the best and mean fitness values during the GWS generations.

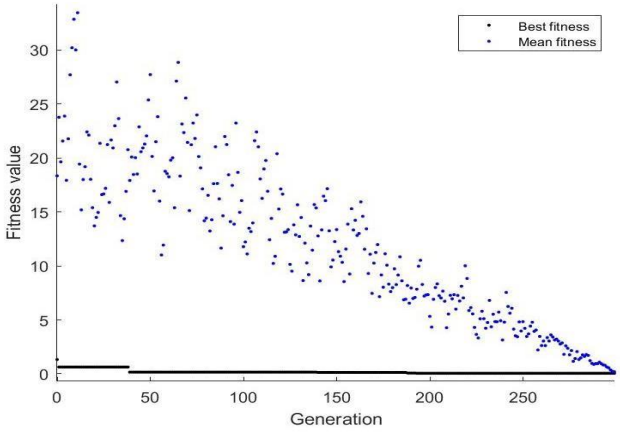

Figure 7: The best and mean fitnesses during the GA generations to find the best weight coefficients of the GWS

July-August 2020
ISSN: 0193-4120 Page No. 3035 - 3052

VI. CONCLUSION

In this work, a new and full scheme for classifying various essential brain activities of motor, vision and prefrontal was designed. Three views of fMRI images were employed (the X_axis, Y_axis and Z_axis). It was investigated that increasing the viewing information of brain activities can lead to achieve better performance.

The designed structure involved many processing stages. Firstly, collecting the fMRI images of vision, movement and prefrontal brain cortices activities by using the SPM to apply the spatial pre-processing, temporal pre-processing and statistical analyses. Then, utilizing the GIFT to identify the brain activity areas in each image. As mentioned, comprehensive study was provided by exploiting the orthogonal presentations of (X_axis, Y_axis and Z_axis). Secondly, preparing all the employed images by applying the pre-processing of cropping. Moreover, the images will be partitioned into two phases: training and testing. Thirdly, proposing three DL networks, each for a specific view. These are the XCM, YCM and ZCM. These models were designed, evaluated and performed in the case of vision, movement and prefrontal brain activities classification. Extensive experiments were exploited to assess their parameters in the case of obtaining the highest accuracies. Fourthly, applying a decision fusion by using the suggested GWS rule to the outputs of all the DL models. The GWS is based on the GA, it has the capability to find the best coefficients for the outcomes of the XCM, YCM and ZCM that could further increase the successfulness of the classification decision.

After extensive experiments, the accuracies of 91.67%, 89.88% and 91.67% have been obtained for the XCM, YCM and ZCM, respectively. In addition, the accuracy has been raised to 97.22% by applying a GA fusion method with the suggested GWS rule. The subject of this work can help doctors, researchers and medical careers in understanding the personal neurons activities of different brain portions.

REFERENCES

[1] X. Fan and M. Henry , "A Brief History of Simulation Neuroscience", *Frontiers in neuroinformatics* , vol. 13, no. 32, 2019.

[2] L. Kristin, R. Ahmad, and D. Roy (ed.), "Neuroimaging Genetics: Principles and Practices", *Oxford University Press*, 2016.

[3] M. A. Renner, M. Martin, C. A. Wenzel, D. Bicknell, L. S. Hurles, M. E. Knoblich, and J. A. Lancaster, "Cerebral Organoids Model Human Brain Development and Microcephaly", *Nature*, vol. 501(7467), pp. 373-379., 2013.

[4] A. Sandra, "Discovering the brain," *National Academies Press*, 1992.

[5] K. Suresh, "Psychoradiology", *Neuroimaging Clinics*, vol. xv, no. 30.1, 2020.

[6] H. Kaynig, V. Botha, C. P. Bruckner, S. Dercksen, V. J. Hege, H. C. Roerdink, and J. B. Pfister, "Visualization in Connectomics", *Scientific Visualization , arXiv*, vol. DOI: 10.1007/978, no. 21, 2014.

[7] W. Lori , "Functional Magnetic Resonance Imaging (fMRI): An Invaluable Tool", *Translational Neuroscience*, 2012.

[8] M. E. Bachert, P. Meyerspeer, M. Moser, E. Nagel, A. M. Norris, D. G. Zaiss, and M. Ladd, "Pros and Cons of Ultra-High-field MRI/MRS for Human Application", *Progress in nuclear magnetic resonance spectroscopy*, vol. 109, no. 15, 2018.

[9] K. Deping and H. Lianghua, "Classification on ADHD with Deep Learning," *International Conference on Cloud Computing and Big Data. IEEE*, pp. 27-32, 2014.

[10] J. You, X. Wu, W. Guillen, M. R. Cabrerizo, M. Sullivan, J. Adjouadi, and M. Wang, "Classification of fMRI Patterns—a Study of the Language Network Segregation in Pediatric Localization Related Epilepsy ", *Human brain mapping*, vol. 4, no. 35, 2014.

[11] N. F. M. Htike, Z. Z. Rashid, N. K. A. M. Suhaimi, "Studies on Classification of fMRI Data Using Deep Learning Approach ," *ARPN Journal of Engineering and Applied Sciences*, vol. 10, no. 21, 2015.

[12] J. Regina, B. Krisztian and Z. V.Meszlényi, "Resting State fMRI Functional Connectivity-Based Classification Using a Convolutional Neural Network Architecture" , *Frontiers in neuroinformatics* , 2017.

[13] D. Wei, Z. Zhou, Y. Li, G. Zhang, X. Han, W. Wen, "Deep Learning Methods to Process fMRI Data and Their Application in the Diagnosis of Cognitive Impairment: a Brief Overview and our Opinion," *Frontiers in neuroinformatics*, vol. 12, no. 23, 2018.

[14] A. Insabato, A. Sanja, S. Kühn, D. Mantini,G. Deco, M. Gilson V. Pallares, "Extracting Orthogonal Subject- and Condition-Specific Signatures from fMRI Data Using Whole-Brain Effective Connectivity," *NeuroImage*,

July-August 2020
ISSN: 0193-4120 Page No. 3035 - 3052

2018.

[15] Y. Kazemi , and S. Houghten, "A deep learning pipeline to classify different stages of Alzheimer's disease from fMRI data", *IEEE Conference on Computational Intelligence in Bioinformatics and Computational Biology (CIBCB)*, 2018.

[16] R. V. Rullen and L. Reddy, "Reconstructing faces from fMRI patterns using deep generative neural networks," *Commun. Biol*, vol. 2, no. 1, 2019.

[17] A. Heldmann, M. Mertins, A. Brabant, G. Nolde, J. M. Jauch-Chara, K. Münte, and T. F. Al-Zubaidi, "Impact of Hunger, Satiety, and Oral Glucose on the Association between Insulin and Resting-state Human Brain Activity," *Frontiers in human neurosc*, vol. 13, no. 62, 2019.

[18] L. Karmakar, S. Misra, C. Dash, S. R. Pani, "Multilevel Classification Framework of fMRI Data: A Big Data Approach. In Big Data Analytics for Intelligent Healthcare Management", *Academic Press*, 2019.

[19] P. Khaire, P. Kumar and J. Imran," Combining CNN streams of RGB-D and Skeletal Data for Human Activity Recognition", *Pattern Recognition Letters*, 2018.

[20] R. R. Omar, T. Han, S. A. Al-Sumaidaee and T. Chen, "Deep Finger Texture Learning for Verifying People.," *IET Biometrics*, vol. 1, no. 8, 2018.

[21] C. L. Huang and C. Y. Tsai, "A hybrid SOFM-SVR with a Filter-based Feature Selection for Stock Market Forecasting", *Expert Systems with Applications*, vol. 2, no. 36, 2009.

[22] J. Brownlee, "A Gentle Introduction to Padding and Stride for Convolutional Neural Networks", 2019.

[23] A. Khan, A. Sohail, U. Zahoora and A. S. Qureshi, "A Survey of the Recent Architectures of Deep Convolutional Neural Networks", *Artificial Intelligence Review*, 2019.

[24] M. Ahmed, F. Girshick, R. Zitnick, L. Batra, and D. Cogswell, "Reducing overfitting in deep networks by decorrelating representations", *arXiv preprint arXiv:1511.06068*, 2015.

[25] Ifu Aniemeka. (2017) A Friendly Introduction to Convolutional Neural Networks. [Online]. https://hashrocket.com

[26] Q. Zhao, S. Lyu, B. Zhang, and W.Feng, "Multiactivation pooling method in convolutional neural networks for image recognition", *Wireless Communications and Mobile Computing, 2018*, 2018.

[27] R. R. O. Al-Nima, "Signal Processing and Machine Learning Techniques for Human Verification Based on Finger Textures" , *Newcastle University*, 2017.

[28] M. T. Al-Kaltakchi, R. R. Omar, H. N. Abdullah, T. Han and J. Chambers, , "Finger Texture Verification Systems Based on Multiple Spectrum Lighting Sensors With Four Fusion Levels", *Iraqi Journal of Information & Communications Technology*, vol. 3, no. 1, 2018.

[29] H. Stryhn, P. Lind, M. T. Collins, "Conditional Dependence between Tests Affects the Diagnosis and Surveillance of Animal Diseases", *Preventive veterinary medicine*, vol. 1, no. 45, 2000.

[30] H. Yan-Yan, Z. Dong-Hua, "Fault Diagnosis Techniques for Dynamic Systems", *Acta Automatica Sinica*, vol. 6, no. 35, 2009.

[31] J. T. Huang, M. H. Wang, W. J. Li and B. Gu, "Multiple classifier fault diagnosis system based on dynamic weight", *Dianzi Xuebao(Acta Electronica Sinica)*, vol. 4, no. 40, 2012.

[32] L. Sun, C. Z. Han, J. J. Shen and N. Dai, "Generalized Rough Set Method for Ensemble Feature Selection and Multiple Classifier Fusion", *Acta Automatica Sinica*, vol. 3, no. 34, 2008.

[33] M. Woźniak, M. Graña, and E. Corchado, "A survey of Multiple Classifier Systems as Hybrid Systems", *Information Fusion*, no. 16, 2014.

[34] M. De-la-Torre, E. Granger, P. V. Radtke, R. Sabourin and D. O. Gorodnichy, "Partially-supervised Learning from Facial Trajectories for Face Recognition in Video Surveillance", *Information fusion*, no. 24, 2015.

[35] M. Panda, A. Abraham and M. R. Patra, "Hybrid Intelligent Systems for Detecting Network Intrusions", *Security and Communication Networks*, vol. 8, no. 16, 2015.

[36] X. Yang, "Chapter 5 - Genetic Algorithms", in *Nature-Inspired Optimization Algorithms*. Tiew On Ting, Chien , 2014, pp. 77-87.

[37] S. Datta, "Efficient Genetic Algorithm on Linear Programming Problem for Fittest Chromosomes", *Journal of Global Research in Computer Science*, vol. 3, no. 6, 2012.

[38] A. J. and P. D. Sheth Umbarkar, "Crossover Operators in Genetic Algorithms: a Review", *CTACT journal on soft computing*, vol. 1, no. 6, 2015.

July-August 2020
ISSN: 0193-4120 Page No. 3035 - 3052

[39] M. T. Medaglia, F. Tecchio, S. Seri, G. Lorenzo, P. M. Rossini, and C. Porcaro, "Contradiction in Universal and Particular Reasoning", *Human brain mapping*, vol. 12, no. 30, 2009.

[40] C. Porcaro, M. T. Medaglia, N. Ja. Thai, S. Seri, P. Rotshtein, and F. Tecchio, "Contradictory Reasoning Network: An EEG and fMRI", *PloS one* , vol. 3, no. 9, 2014.

[41] R. R. AL-Nima, M. T. Al-Kaltakchi, S. A. Al-Sumaidaee, S. S. Dlay, W. L Woo, T. Han, and J. A. Chambers, "Personal verification based on multi-spectral finger texture lighting images", *IET Signal Processing*, vol. 9, no. 12, 2018.

[42] R. R. Al-Nima, S. S. Dlay, W. L. Woo, "A new approach to predicting physical biometrics from behavioural biometrics", *International Journal of Computer, Information, Systems and Control Engineering*, vol. 8, no. 11, 2014.

[43] R. R. O. Al-Nima, S. S. Dlay, W. L. Woo, and J. A. Chambers, "Efficient Finger Segmentation Robust to Hand Alignment in Imaging with Application to Human Verification", *5th IEEE International Workshop on Biometrics and Forensics (IWBF)*, 2017.

[44] R. R. O. Al-Nima, "Design a biometric identification system based on the fusion of hand geometry and backhand patterns", *Iraqi Journal of Statistical Science*, 2010.

[45] M. A. Abdullah, R. R. Al-Nima, S. S. Dlay, W. L. Woo, and J. A.Chambers, J. A., "Cross-spectral Iris Matching for Surveillance Applications", *Springer, Surveillance in Action Technologies for Civilian, Military and Cyber Surveillance, Chapte5*, 2018.

[46] R. R. O. Al-Nima, "Human authentication with earprint for secure telephone system", *Iraqi Journal of Computers, Communications, Control and Systems Engineering IJCCCE*, vol. 2, no. 12, 2012.

[47] F. H. Abdulraheem. M. Y. Al-Ridha, and R. R. O. Al-Nima, "Using Hand-Dorsal Images to Reproduce Face Images by Applying Back propagation and Cascade-Forward Neural Networks", *2nd International Conference on Electrical, Communication, Computer, Power and Control Engineering (ICECCPCE19)*, 2019.

[48] R. R. O. Al-Nima, H. N. Abdullah, T. Han and J. A. Chambers, M. T. Al-Kaltakchi, "Finger texture verification systems based on multiple spectrum lighting sensors with four fusion levels", *Iraqi Journal of Information & Communications Technology*, vol. 1, no. 3, 2018.

[49] M. S. Majeed, R. R. O. Al-Nima and M. R. Khalil, "Personal identification with iris patterns", *AL-Rafidain Journal of Computer Sciences and Mathematics, College of Computer Sciences and Math / University of Mosul / Iraq*, vol. 1, no. 6, 2009.

[50] R. R. Omar Al-Nima, M. Y. Al-Ridha and F. H. Abdulraheem, "Regenerating face images from multi-spectral palm images using multiple fusion methods", *TELKOMNIKA*, vol. 6, no. 17, 2919.

[51] R. R. O. Al-Nima, N. A. Al-Obaidy and L. A. Al-Hbeti, "Segmenting Finger Inner Surface for the Purpose of Human Recognition", *2nd International Conference on Engineering Technology and its Applications (IICETA), IEEE*, 2019.

[52] T. Han, T. Chen, R. R. O. Al-Nima "Road Tracking Using Deep Reinforcement Learning for Self-driving Car Applications", In: R. Burduk, M. Kurzynski and M. Wozniak (eds)", *Progress in Computer Recognition Systems, Progress in Computer Recognition Systems, CORES 2019, Advances in Intelligent Systems and Computing, Springer*, Cham, 2020.

[53] M. M Abuqadumah, M. A. Ali, and R. R. Al-Nima, "Personal Authentication Application Using Deep Learning Neural Network", *in 16th IEEE International Colloquium on Signal Processing & its Applications (CSPA), Langkawi, Malaysia*, 2020.

[54] R. R. O. Al-Nima and S. Kasim, "Picture Recognition by Using Linear Associative Memory Neural Network", *Tikrit Journal of Pure Science*, vol. 3, no. 13, 2008.

[55] A. Hamed, L. H. Albak, and R. R. O. Al-Nima, "Design Security System based on Arduino", *TEST Engineering & Management, The Mattingley Publishing Co., Inc*, vol. 82, no. pp. 3341-3346, 2020.

[56] L. H. Albak, A. H. S. Hamdany and R. R. O. Al-Nima, "Wireless Waiter Robot", *TEST Engineering & Management, The Mattingley Publishing Co., Inc*, vol. 81, no. pp. 2486-2494, November-December 2019.

[57] R. R. Al-Nima, T. Han, T. Chen, S. Dlay , and J. Chambers, "Finger Texture Biometric Characteristic: a Survey," *arXiv preprint arXiv*, 2020.

[58] M. Y. Al-Ridha, R. R. O. Al-Nima, and A. S. Anaz, "Adaptive Neuro-Fuzzy Inference System for Controlling a Steam Valve", *IEEE 9th International Conference on System Engineering and Technology (ICSET)*, Shah Alam, Malaysia 2019.

[59] J. Xie, R. Liu, J. Luttrell IV, and C. Zhang , "Deep learning based analysis of histopathological images of

July-August 2020
ISSN: 0193-4120 Page No. 3035 - 3052

breast cancer", *Frontiers in genetics*, 2019.